International Journal of NanoScience and Nanotechnology.
ISSN 0974-3081 Volume 7, Number 1 (2016), pp. 1-17

http://www.irphouse.com

Nanostructured Detector Technologies for Optical Sensing Applications

Ashok K. Sood, Roger E. Welser, John W. Zeller and Yash R. Puri
Magnolia Optical Technologies Inc.,
52-B Cummings Park, Suite 314, Woburn, MA 01801

Jay S. Lewis
DARPA/MTO, 675 North Randolph Street,
Arlington, VA 22203

Nibir K. Dhar
Night Vision & Electronics Sensors Directorate,
10221 Burbeck Road Fort Belvoir, VA 22060

Priyalal Wijewarnasuriya
Army Research Laboratory, 2800 Powder Mill Road,
Adelphi, MD 20783

Abstract

Optical sensing technology is critical for optical communication, defense and security applications. Advances in optoelectronics materials in the UV, Visible and Infrared, using nanostructures, and use of novel materials such as CNT and Graphene have opened doors for new approaches to apply device design methodology that are expected to offer enhanced performance and low cost optical sensors in a wide range of applications.

This paper is intended to review recent advancements and present different device architectures and analysis. The chapter will briefly introduce the basics of UV and Infrared detection physics and various wave bands of interest and their characteristics [1, 2]

We will cover the UV band (200-400 nm) and address some of the recent advances in nanostructures growth and characterization using ZnO/MgZnO based technologies and their applications. Recent advancements in design and development of CNT and Graphene based detection technologies have shown promise for optical sensor applications. We will present theoretical and experimental results on these device and their potential applications in various bands of interest.

ZnO / MgZnO Nanostructures for UV Applications

Zinc oxide (ZnO) is a unique wide bandgap biocompatible material system exhibiting both semiconducting and piezoelectric properties that has a diverse group of growth morphologies. Bulk ZnO has a bandgap of 3.37 eV that corresponds to emissions in the ultraviolet (UV) spectral band [3]. Highly ordered vertical arrays of ZnO nanowires (NWs) have been grown on substrates including silicon, SiO_2, GaN, and sapphire using a metal organic chemical vapor deposition (MOCVD) growth process [3]. The structural and optical properties of the grown vertically aligned ZnO NW arrays have been characterized by scanning electron microscopy (SEM), X-ray diffraction (XRD), and photoluminescence (PL) measurements [3-6].

Compared to conventional UV sensors, detectors based on ZnO NWs offer high UV sensitivity and low visible sensitivity, and are expected to exhibit low noise, high quantum efficiency, extended lifetimes, and have low power requirements [7-8]. The Photoresponse switching properties of NW array based sensing devices have been measured with intermittent exposure to UV radiation, where the devices were found to switch between low and high conductivity states at time intervals on the order of a few seconds. Envisioned applications for such sensors/FPAs potentially include defense and commercial applications [9].

Zinc oxide is a versatile functional material that provides a biocompatible material system with a unique wide direct energy band gap and exhibits both semiconducting and piezoelectric properties. ZnO is transparent to visible light and can be made highly conductive by doping. Bulk ZnO has a bandgap of 3.37 eV that includes emissions in the solar blind ultraviolet (UV) spectral band (~240-280 nm), making it suitable for UV detector applications [3]. Over this wavelength range, solar radiation is completely absorbed by the ozone layer of the earth's atmosphere, so the background solar radiation at the earth's surface is essentially zero. This enhances the capability of UV sensors in missile warning systems to detect targets such as missile plumes and flames emitting in this region.

ZnO is the basis for the one of the richest families of nanostructures among all materials taking into accounts both structure and properties. ZnO growth morphologies have been demonstrated for nanowires, nanobelts, nanocages, nanocombs, nanosprings, nanorings, and nanohelixes [3]. The development of ZnO nanowire (NW) based UV detectors offers high UV sensitivity and low visible sensitivity for missile warning related applications. Demonstration of devices using single ZnO NW strands has been widely reported in literature [3-12]. However, the development of reliable 2D arrays of aligned ZnO NWs has proven more challenging. The demonstration of reliable 2D arrays requires (1) correlation of growth process and growth parameters with the material quality of ZnO NWs, (2) correlation of the electrical and optical performance with growth parameters and fabrication processes, and (3) addressing system design challenges [13-14].

With conventional NW growth methods including electrochemical deposition, hydrothermal synthesis, and molecular beam epitaxy (MBE), it is generally difficult to scale up and control NW growth. Electrochemical deposition is well suited for large scale production but does not allow control over the NW orientation. Hydrothermal synthesis is a low temperature and low-cost process that allows growth

of NWs on flexible substrates without metal catalysts, but the direction and morphology of the NWs cannot be well-controlled with this method [4-6].
The MBE method allows monitoring of the structural quality during NW growth; however, this type of synthesis often requires use of metal catalysts as a seed layer [6], which introduces undesired defects to the structure, decreasing the crystal quality [8-12]. Chemical vapor deposition (CVD) also requires catalysts at the NW tips, and using this method the tips of the grown NWs were observed to be flat, with vertical alignment.

Characterization of ZnO NWs arrays grown on the various substrates

The samples were characterized by scanning electron microscopy (SEM) utilizing a Quanta FEG 250 system, and X-ray diffraction (XRD) using Bruker D-8 Advance X-ray diffractometer with a wavelength of 1.5406 Å corresponding to the Cu Kα line. In addition, photoluminescence (PL) measurements were performed at room temperature using a Linconix HeCd UV laser emitting at a wavelength of 325 nm. A Si detector in conjunction with at lock-in amplifier and chopper were used to measure the PL from the beam reflected off the sample at the output over the desired wavelength range [14-16].

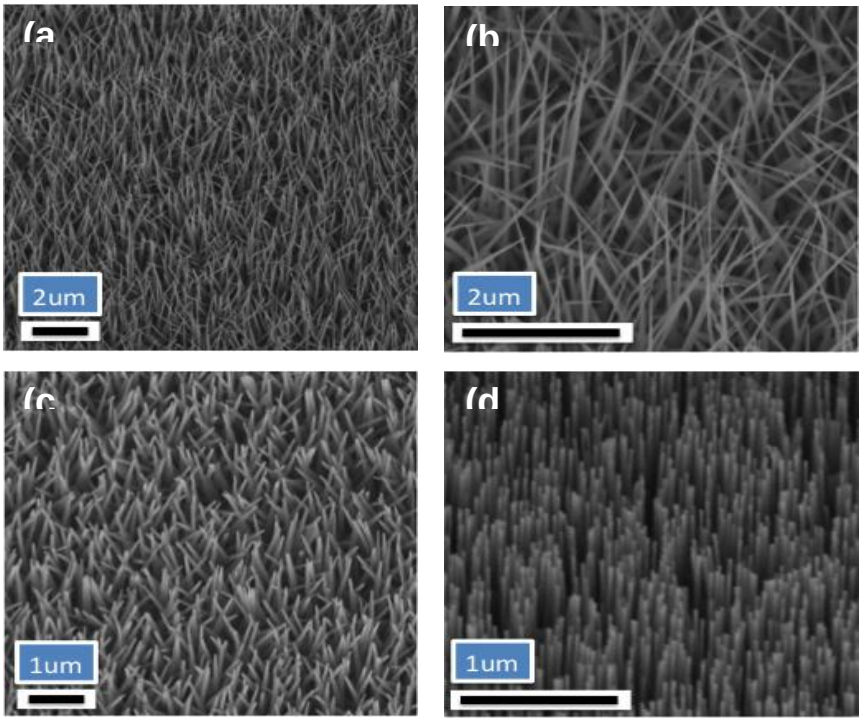

Figure 1: Scanning electron microscope (SEM) images of NWs grown on the various substrates taken at room temperature, showing NWs grown on (a) ZnO/sapphire; (b) ZnO/SiO_2/p-Si; (c) ZnO/p-Si; and (d) ZnO/GaN/sapphire.[16]

SEM was performed to explore the NWs morphology. Figure 1 shows the synthesized ZnO NWs on the various substrates, which can be generally seen to have uniform distribution density. The ZnO NWs grown on sapphire [Figure 1(a)] had approximate diameters of 50-70 nm and lengths in the range of 1-2 µm. NWs grown on SiO_2 [Figure 1(b)] had diameters of 150-200 nm and lengths of 1-2 µm, and were the least vertically oriented and associated with a relatively high lattice mismatch. NWs grown on the Si (111) substrate [Figure 1(c)] had a slightly random orientation, also having diameters in the range of 150-200 nm and lengths from 1-2 µm. Finally, the NWs grown on GaN [Figure 1(d)] showed strong vertical orientation, with diameters of 20-40 nm and lengths of 0.7-1.0 µm [16].

Figure 2 shows the XRD pattern for the ZnO NWs grown on p-Si, GaN, and SiO_2 substrates [6]. The inset of Figure 2 shows dominant peaks related to ZnO (002). The peak at 34º (2θ) for ZnO grown on p-Si and SiO_2 substrates incorporated the overlapping of ZnO NWs (002) and ZnO thin film (002). An additional diffraction peak associated with GaN was present for the GaN/sapphire substrate. ZnO NWs oriented along the (002) direction had full-widths at half maxima (FWHM) and c-lattice constants of 0.0498 (θ) and 5.1982 Å at 34.48° (2θ) for p-Si, 0.0497(θ) and 5.1838 Å at 34.58° (2θ) for GaN, 0.0865(θ) and 5.1624° at 34.38º (2θ) for SiO_2, and 0.0830˚(θ) and 5.2011 Å at 34.46º (2θ) for sapphire.

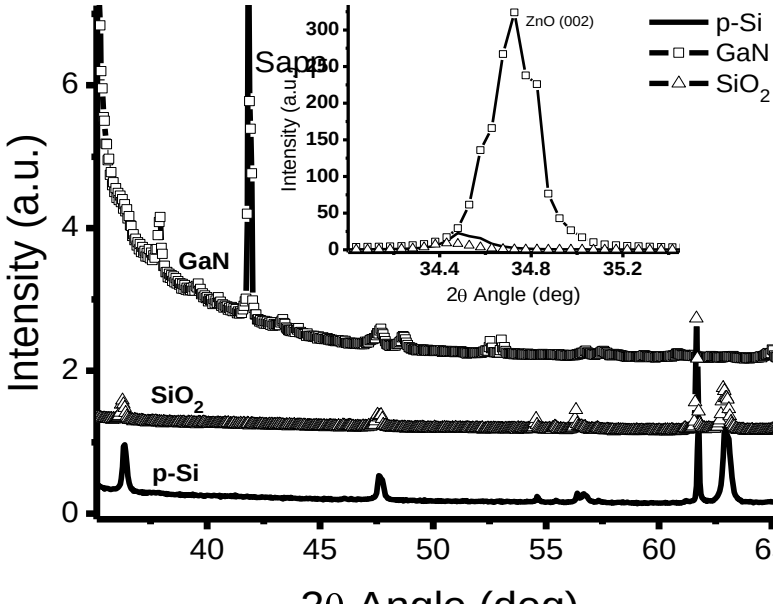

Figure 2:X-ray diffraction (XRD) of ZnO NWs grown using MOCVD on p-Si (solid), GaN/sapphire (square) and SiO_2 (triangle). The inset shows the ZnO peak associated with ZnO oriented along (002) and GaN [16].

The quality of the ZnO epilayers utilized as seed layers to grow ZnO NWs was also characterized. The ZnO thin films were oriented along (002) and had a maximum at 34.58º with FWHM of 0.0697 (θ) for p-Si, maximum of 34.58º with FWHM of

0.0684 (θ) for GaN, and maximum of 34.43º with FWHM of 0.0557 (θ) for SiO_2. Additional shallow diffraction peaks were observed for NWs grown on p-Si and SiO_2, which are attributed to ZnO (100, 101, 102 and 110) as can be seen from Figure 6. As shown in Figure 7, for ZnO NW growth on sapphire major peaks were observed for ZnO (002) at 34.46° (2θ) and Al_2O at 37.91° (2θ), with a minor peak for ZnO (101) at 36.34° (2θ).

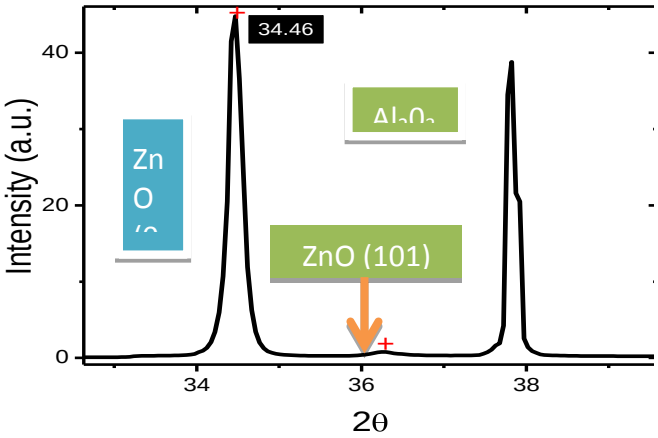

Figure 3: XRD of ZnO NWs grown using MOCVD on sapphire [16]

Photoluminescence (PL) Measurements

Figure 4 shows the PL spectra for ZnO NWs grown on p-Si, GaN, and SiO_2 substrates [6]. The room temperature PL measurements were performed using a ~280 nm light source. Single peaks located at 380 nm having a FWHM of 14.69 nm and at 378 nm having a FWHM of 15 nm were observed for p-Si and SiO_2 substrates, respectively, corresponding to the recombination of excitons through an exciton-exciton collision process [14-16].

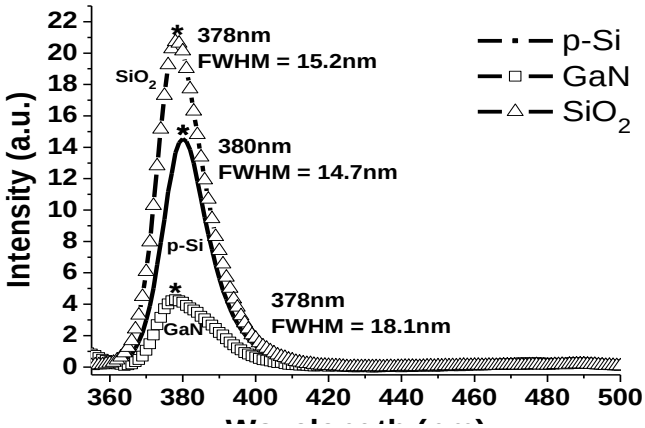

Figure 4: Photoluminescence (PL) of ZnO NWs grown on p-Si (100) (solid) with a single peak at 380 nm, GaN (square) with a stronger peak at 378 and SiO_2 (triangle) with a single peak at 378 nm [16].

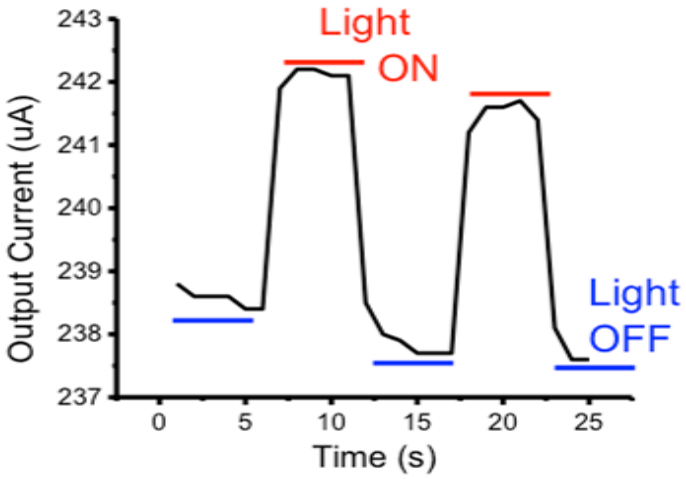

Figure 5: Switching Photoresponse characteristics of ZnO NW device when UV LED source at ~370 nm turned on and off over approximately 10 s intervals[16]

No defects related to Zn or O vacancies were observed, which can be attributed to the confinement of defects at the ZnO thin film/substrate interface. For the ZnO NWs grown on GaN, a predominant peak with a FWHM of 18.18 nm was observed at 378 nm. High stress was evident for ZnO NWs grown on GaN, which can be observed in Figure 2; this can contribute to the broadening of the peak in comparison to p-Si and SiO_2. Shallow peaks identified at 474 nm and 490 nm through Lorentzian decomposition are attributed to oxygen interstitial and oxygen vacancies, respectively [16].

A UV LED lamp acquired from Sensor Electronic Technology Inc. was used to characterize the UV Photoresponse of the ZnO NW arrays [20]. The lamp comprises eight separate AlGaN based UV LEDs in a TO-3 package spanning the 240-370 nm wavelength range, with a customized power supply capable of independently monitoring and controlling the current of all or any of the LEDs. The Photoresponse was determined by first applying voltage between indium contacts on the front and back sides of a Si NW sample and measuring the resulting current in the dark, and then repeating this procedure while the sample was exposed to radiation from a UV LED at a specific wavelength.

Figure 5 shows the on-off switching characteristics of a ZnO vertical array NW device when exposed to radiation at 370 nm. This device was found to switch between low and high conductivity states in approximately 3 s, a faster response than most reported thus far for ZnO NW based UV detectors.

ZnO nanowires based arrays offer high sensitivity and have potential application in UV imaging systems. ZnO nanowire array based UV detectors have no moving parts, high quantum efficiency, extended lifetimes, low noise, low power requirements, and offer high sensitivity.

Nanostructured Detector Technologies for MWIR and LWIR Bands

EO/IR Sensors and imagers using nanostructure based materials are being developed for a variety of Defense Applications. In this section, we will present recent work under way for development of next generation carbon nanostructure based infrared detectors and arrays. We will discuss detector concepts that will provide next generation high performance, high frame rate, and uncooled nano-bolometer for MWIR and LWIR bands [21-24]. The critical technologies being developed include carbon nanostructure growth, characterization, optical and electronic properties that show the feasibility for IR detection. Experimental results on CNT nanostructures will be presented. Further discussion will be provided for the path forward to demonstrate enhanced IR sensitivity and larger arrays.

The microbolometer based on Si-MEMS device structure has been under development for over 20 years with support from DARPA and the US Army. Two most common Si-MEMS based structures utilize VOx and amorphous silicon based technologies. Several companies such as BAE systems and DRS Technologies are developing and producing 17 micron unit cell 640x 480 and larger arrays using VOx [17-20]. Similarly, L3Communications and other groups are developing and producing 640x480 with 17 micron unit cell using amorphous-Silicon technology [19-20].

We will discuss the use of carbon nanostructures for use as the high performance bolometric element of the MWIR and LWIR bands. As part of this effort, we are exploring development of smaller unit cell bolometer .i.e. 5-10 micron unit cell, with higher TCR and higher frequency response in the 1 to 10 KHz range. The feasibility of such an array can open up a larger number of defense and commercial applications. This section will discuss the efforts under way to explore these possibilities.

Calculating the Electrical Response of the CNT Film

To read the temperature that the bolometer pixel reaches after an exposure to infrared radiation, one needs to measure the electrical resistance of the pixel. By comparing this resistance to a look-up table or using the a-priori knowledge of temperature coefficient of resistance, the pixel temperature can be determined. Therefore, in addition to having a large thermal resistance which translates into higher temperature rises, a large temperature coefficient of electrical resistance (TCR) is desirable to achieve a higher temperature resolution Here TCR is defined as the change in electrical resistance per degree Kelvin divided by the absolute electrical resistance measured at the quiescent point, as follows:

$$TCR = \frac{1}{R_e}\frac{dR_e}{dT}$$

Thus, the pixel electrical resistance after it reaches a temperature that is ΔT above its ambient becomes $R_e(T) = R_e(To)(1+TCR)$. Using this relationship, the pixel temperature is calculated.

To obtain a high temperature resolution, a large change in electrical resistance is needed upon heating. To achieve this, a substantial increase either in electron concentration or velocity (for a given electric field) is necessary. And to this end,

materials with junctions where thermionic emission or tunneling are the electrical current bottlenecks offer a good solution. As the tunneling current exponentially rises with temperature, the effective change in their electrical resistance due to temperature becomes large compared to those observed in bulk materials where the change is proportional T^{γ} and γ is generally < 2.

Here, a film of CNTs is proposed as the bolometer pixel material, since it is likely to have large thermal resistance and TCR values simultaneously. Both of these favorable properties are partially owed to the junctions between the tubes. As the electrical current flows along the mat, it needs to jump from one tube to the next where they intersect.

At this intersection, the carriers see a potential barrier that they need to tunnel through which gives rise to exponential increase in current upon heating. Assuming that the electron transport across this barrier is governed by a Fowler-Nordheim-type tunneling or thermionic emission, the expected TCR values can be calculated using the following expression:

$$I = q\int_0^{\infty} T_t(E)v(E)DOS(E)f(E,T)dE$$

Where T_t, v, DOS and f, are the transmission coefficient, thermal velocity, density of states and distribution function, respectively for electrons in the CNT. We perform this calculation a function of barrier height and electric field. The results are shown in figure 6. The figure on the left shows a contour plot of the theoretical values of the TCR for a CNT film.

The TCR is plotted as a function of electric field between the tubes and the barrier height. Theoretical calculations predict an extremely large TCR, which can be attributed to the relatively large barrier height between adjacent CNTs. If a lower barrier height is assumed, on the order of 0.06eV, then a TCR of approximately 2.5% is obtained. It is also worth pointing out that such a large TCR comes at the price of extremely low output currents. The bolometer current densities, as a function of barrier height and electric field are shown in Figure 6, on the right.

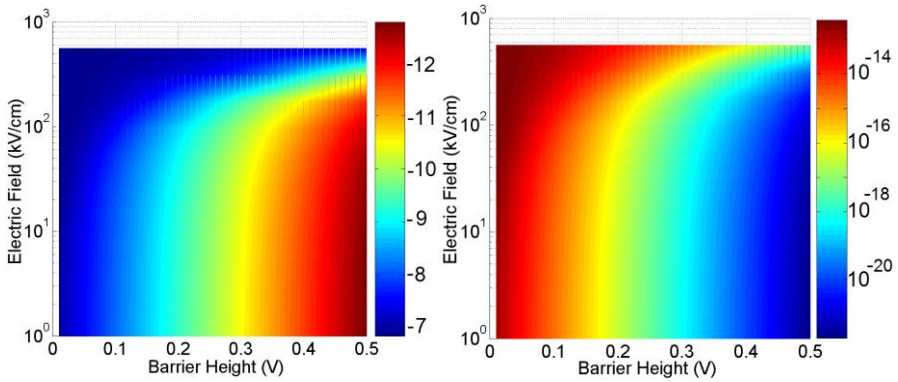

Figure 6: Left figure is a contour plot of TCR versus electric field and barrier height between CNTs of the film. The right figure shows the bolometer current also as afunction of electric field and barrier height. The scales are the color bars on the right of each contour plot in units of %TCR and amperes, respectively [23].

CNT Growth and Charcterization

In this section, we will discuss growth and characterization of carbon nanotubes with single wall (SWCNT) and multiwall (MWCNT) for use as the high performance bolometric element for development of MWIR and LWIR sensitive detector elements.

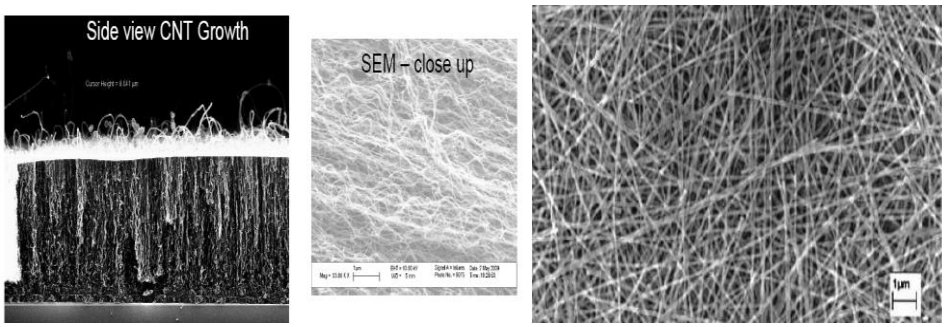

Figure 7: Growth of multiwall CNT forest with the ability to separate the form growth substrate with good length /diameter uniformity and the MWCNT released from the template [24].

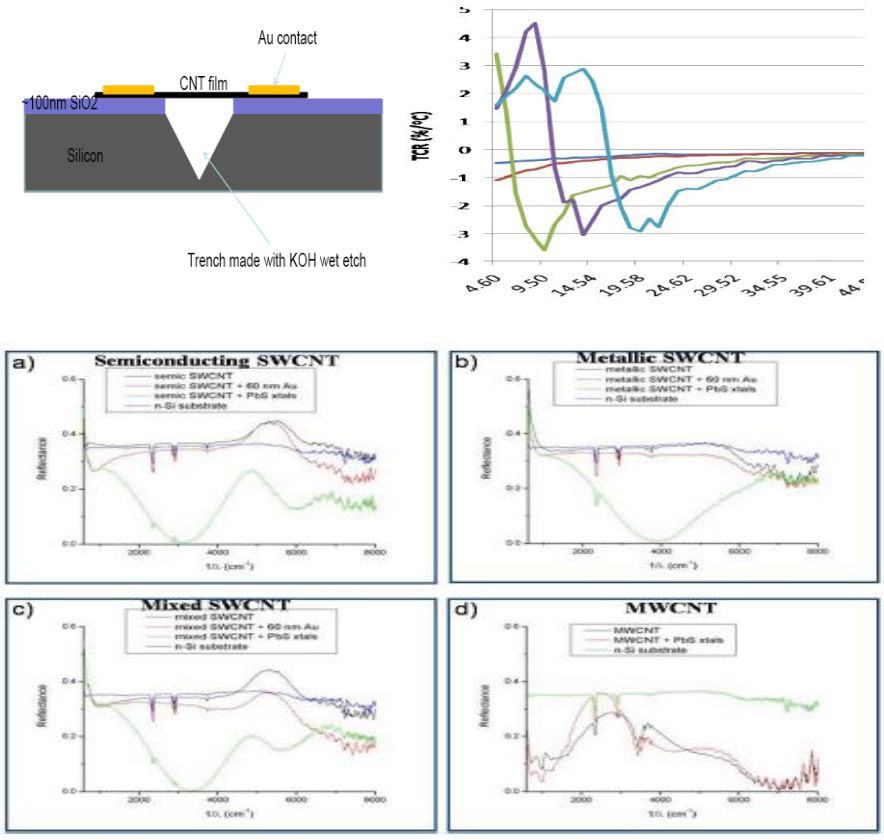

Figure 8: The composite figure shows prototype CNT film bolometer test fixture to evaluate the CNT film quality. Some preliminary data on reflectivity measurements for SWCNT and MWCNT are shown along with preliminary results on TCR measurements [24].

Figure 7 presents growth of dense oriented multi-walled CNT “forest like growth”. The figure shows the CNT growth can be easily separated from the growth substrate. We have shown good length/diameter uniformity. Further work on the growth optimization is underway.

Figure 8 shows the prototype fixture to evaluate the CNT films for bolometric application. This fixture is being used for quick evaluation of both electrical and optical characteristics of the CNT samples. The figure also shows the preliminary results of reflectivity measurements for SWCNT and MWCNT samples with various sample treatments. We have carried out some preliminary measurements of TCR on CNT samples.

Figure 9 shows scanning electron microscopySEM.images of representative MWCNT films in the unsuspendedleft. and suspended .right. forms, respectively. Unlike theirSWCNTcounterparts,the MWCNT films contain substantialuncovered substrate areas. In addition,some minor deformation of recess is visible on suspendedMWCNT films, which is similar to the SWCNT film case inthe same thickness range.Figure 9.b includes a transmissionelectron microscopy .TEM. image of a representativeindividual MWCNT, which has a large hollow center of approximately10–11 nm in diameter and contains approximately40–50 CNT shells.

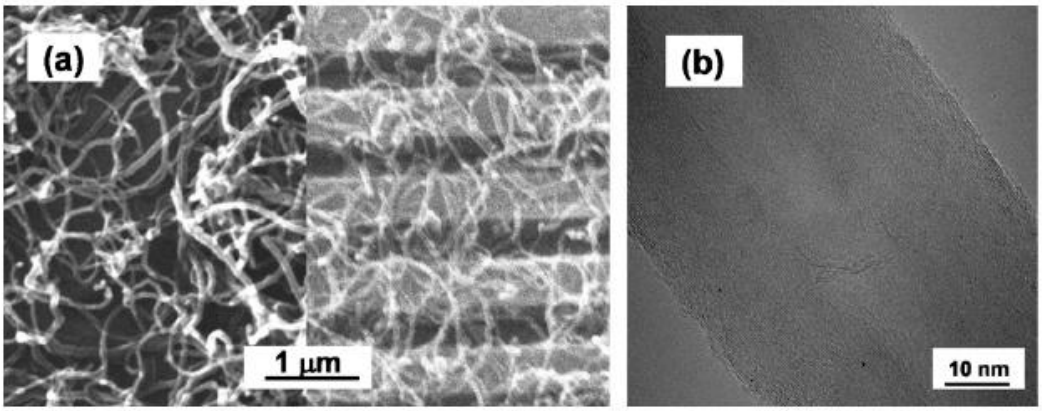

Figure 9: SEM images of unsuspended Left (a). and suspended Right (b).MWCNT films. A TEM image of a representative MWCNT. The shellnumber is estimated to be 40–50 for the MWCNTs [56]

All MWCNT films studied in this work [56] show semi-conductiveresistance-temperature .R-T. behaviors and a representativecurves is depicted in Figure 36.. Nevertheless, the increasein the resistivity of MWCNT films is much less thanthat of SWCNT films with decreasingtemperature, as shownin Figure 11. This is not unexpected considering a much smallerband gap in MWCNTs. The reduced temperature dependencealso implies smaller TCR absolute value in MWCNTs. Forexample, the TCR absolute value at room temperature forMWCNT films isabout

0.07%/K in contrast to .0.17%/Kfor SWCNT films. R-T curve after suspending the MWCNTfilm has been also measured.

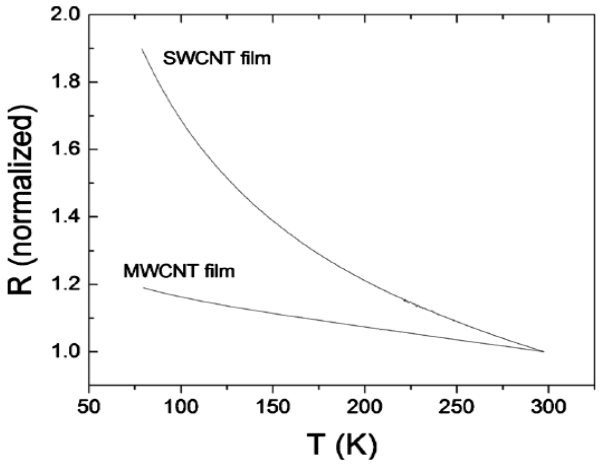

Figure 10: Resistance versus temperatures curves of SWCNT films and MWCNTfilms [25]

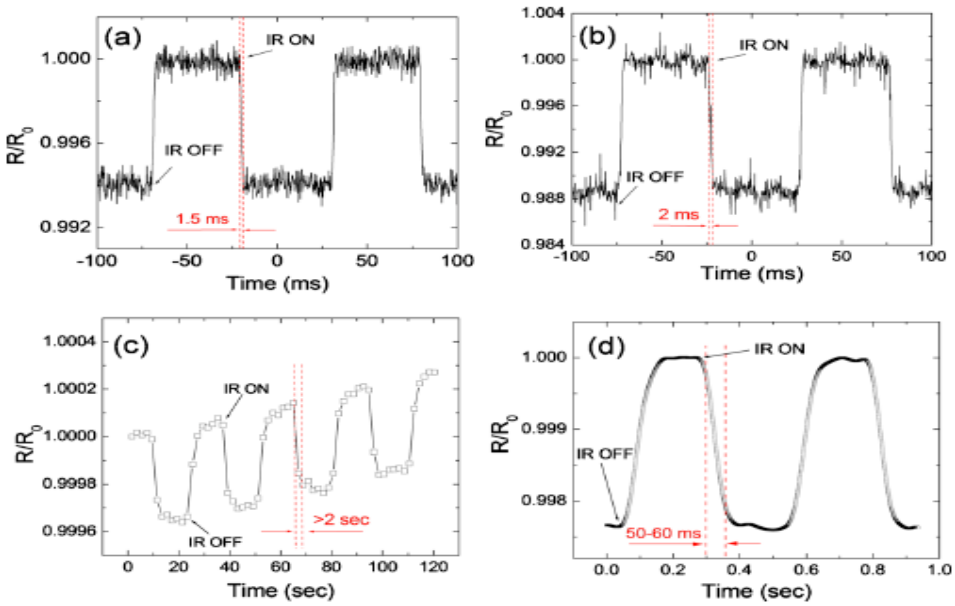

Figure 11: Photoresponse of unsuspendedand suspended CNT films.(a) Unsuspended MWCNTfilm, f=10 Hz, in IR.3 mW/mm2 ; .(b). suspendedMWCNT film, f=10 Hz, in IR.3mW/mm2 ; (c) unsuspendedSWCNT film, f=1/30 Hz, in IR.3.5 mW/mm2 ; and (d) suspended SWCNT film, f=2 Hz, in IR.3.5 mW/mm2 [25].

Figure 11 compares the Photoresponse R/R0 of MWCNTfilms in unsuspended (a) andsuspended (b) cases, where $R_0$is the sample resistance before IR radiation was turned onand the change in the resistance caused by IR radiation isdefined as .R=R-R_0. For comparison, the results of theirSWCNT counterparts are also included in Figure 11(c).unsuspendedand Fig.11(d). suspended..

Two major differencesare visible between MWCNT and SWCNT films, a significantlyhigher .R/R_0 and a much shorter response time in thecases of MWCNT. The .R/R_0 for MWCNT samples is typicallyin the range of a few percent, which is more than oneorder of magnitude higher than that of suspended SWCNTfilms and two orders of magnitude higher than the unsuspendedSWCNT films at a comparable IR power.

Consideringa lower TCR absolute value in MWCNTs, the much enhancedPhotoresponse of MWCNT films should be attributedto the naturally suspended inner CNT shells, which may providean ideal configuration to enhance the bolometric effectby improving light absorption and reducing thermal link.Physical suspension of the films in both MWCNT .Fig. 12.(b) and SWCNT .Fig. 12(d.) cases results in a further improvementof .R/R_0 as compared to their unsuspended counterparts.The improvement is, however, much more pronounced in suspended cases [25].

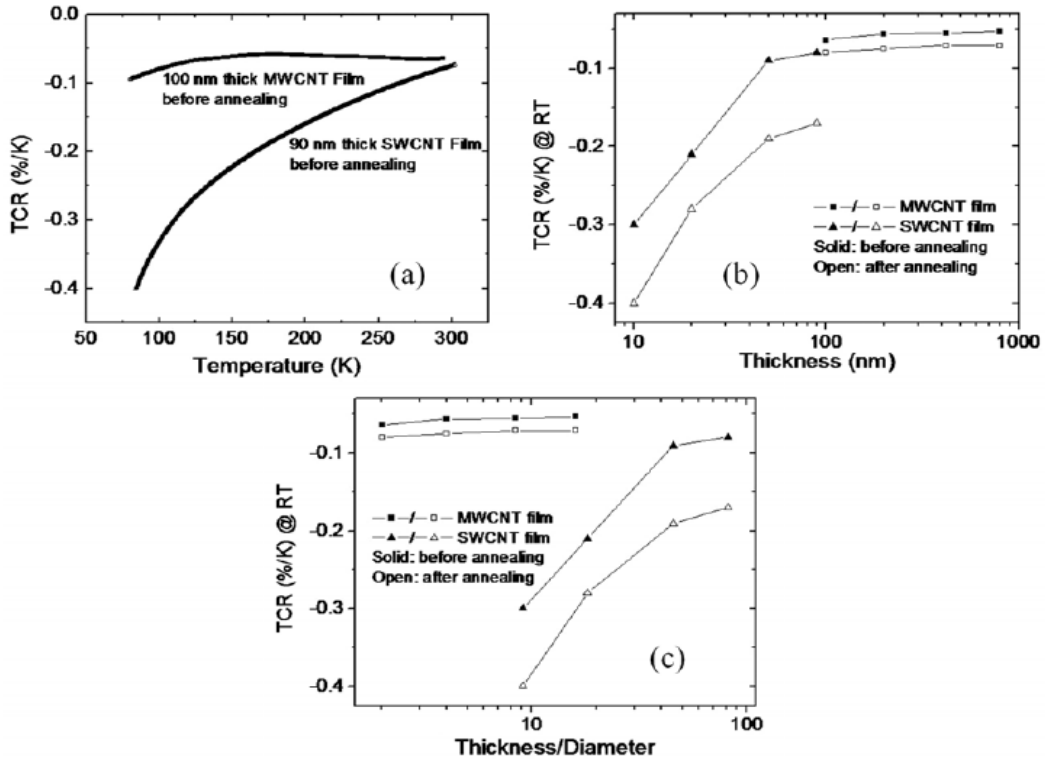

Figure 12: TCR as function of temperature for a 90 nm thick MWCNT film (a) and a 100 nm thick MWCNT film before annealing. (b) TCRversus thickness for MWCNT and SWCNT films with different thicknesses. (c) TCR versus thickness/diameter ratios for SWCNT andMWCNT films [26].

We have also shown the results of TCR as function of temperature in figure 13, for a 90 nm thick MWCNT film (a) and a 100 nm thick MWCNT film before annealing. (b) TCRversus thickness for MWCNT and SWCNT films with different thicknesses. (c) TCR versus thickness/diameter ratios for SWCNT andMWCNT films [26].

We have discussed recent efforts for modeling CNT based bolometer and the experimental work for development of next generation carbon nanostructure based infrared detectors and arrays. Our goal is to develop high performance, high frame rate, and uncooled nano-bolometer for MWIR and LWIR bands. We also discussed CNT growth system and its capability to grow samples of various orientations. We have also presented recent results on SWCNT and MWCNT samples that show promise for use of CNT for developing next generation high performance small pixel bolometer arrays.

Graphene Use in Electro-Optical Devices

Infrared (IR) detectors can be separated into two separate categories: either thermal-based IR detection or photon-based detection.[25] In thermal-based detectors, the incident IR radiation is absorbed raising the temperature of the material.[25] The raised temperature affects some temperature dependent property of the material; for pyrometers this is a change in electrical polarization, while for bolometers this is a change in materials resistance.[25] Another more recent study utilized the photothermoelectric effect in graphene to create a net electric field due to electron diffusion into dissimilar metal contacts.[9] Photon-based detectors utilize band gap-based detection with the arriving photon being absorbed and utilized to promote electron hole pairs to create a photocurrent.[25] The photon-based detectors can be tuned to certain wavelengths by creating a quantum well structure.[25] Photon based IR absorbers are characterized by having fast absorption response but usually require cooling due to thermal effects while thermal-based IR detectors have high responsivity over a large wavelength and can be utilized at room temperature but normally have slow absorption response.[25] This is where utilizing a graphene based sensing element is attractive due to the high mobility with little temperature sensitivity making it ideal for IR detectors.[2]

Several groups have attempted to integrate graphene into IR detectors. The groups have tried both photon and the thermal-based absorption methods.[9, 26-28] For photon-based absorption methods the main focus has been the opening of a band gap through geometric modification.[9, 26] One group utilized bilayer graphene to open a small band gap which is sensitive to thermalization requiring cooling to 5K for operation.[26]

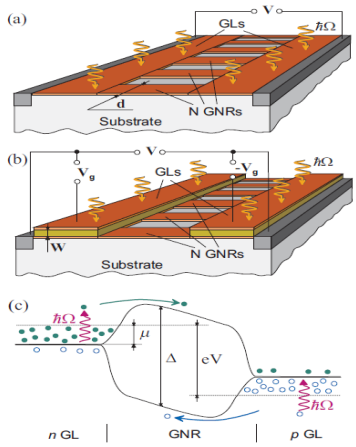

Figure 18: The utilization of graphene nanoribbons to open a small bandgap which is enhanced through the use of p and n type graphene contacts [26]

Another group utilized an array of aligned graphene nanoribbons as shown in Figure 18 to open up a small band gap which has significant difficulties in fabrication and noise properties from the nanoribbon edges.[26] Groups that have tried thermal-based IR detectors seem to have created more novelty, with one group utilizing multiple vertically aligned graphene flakes, while another group utilized a resonant structure of 2 graphene sheets separated by a dielectric to tune the photon wavelength of absorption as shown in Figure 19.[27]

Finally another group utilized the photothermoelectric effect as shown in Figure 20 to induce an electric current in graphene due to electric gating or dissimiliar metal contacts.[9, 27, 28] The bolometer utilizing vertically aligned graphene sheets used distance based tunneling between sheets for the bolometric effect, which is sensitive to contamination between sheets and alignment of the graphene flakes making reproduction difficult.[28]

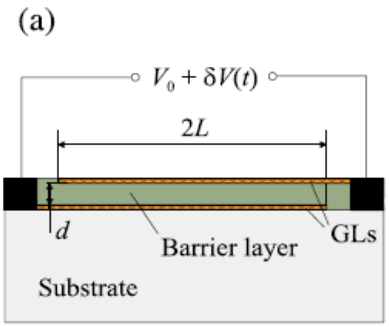

Figure 19: Phonon resonance based IR detector [27]

The resonance based IR detector shown in Figure 19 utilizes the phonon resonance of two separate graphene sheets separated by a dielectric allowing for the tuning of wavelength detection based upon separation distance, but the fabrication is difficult requiring pristine graphene and no trapped states in the oxide which would both modify the resonant frequency and could possibly contaminate the detector out of detection range.[27]

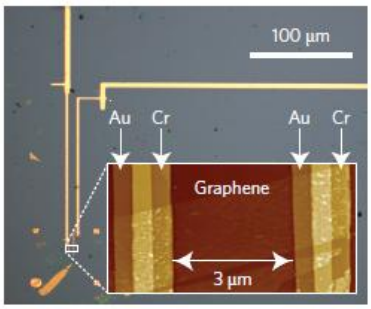

Figure 20: Image of a detector based upon the photothermoelectric effect [9]

The photothermoelectric effect detector shown in Figure 20 is relatively straight forward with contamination only affecting the speed of the detector and the noise only susceptible to trap states of the insulating oxide that the graphene is transferred onto.[9]

Summary

In this paper, we have discussed recent advances in nanostructured based detector technology, materials and devices for optical sensing applications. We have presented an overview of recent work underway on a variety of semiconductors and advanced materials such as ZnO nanowires and CNT and Graphene for optical sensing applications.

Optical sensing technology is critical for defense and commercial applications including optical communication. Advances in optoelectronics materials in the UV, Visible and Infrared, using nanostructures, and use of novel materials such as CNT and Graphene have opened doors for new approaches to apply device design methodology that are expected to offer enhanced performance and low cost optical sensors in a wide range of applications.

Acknowledgements

The Magnolia authors gratefully acknowledge the DARPA and Navy SBIR Program support for development of nanotechnology based EO/IR detector technology for optical sensor applications.

References

[1] N. K. Dhar. " IR Material Research at the Army Research Laboratory" Invited Keynote Paper, Proceedings of SPIE, Volume 6542, 65420C (2007)

[2] Ashok K. Sood, Robert A. Richwine, Yash R. Puri, Nibir K. Dhar, Dennis L. Polla, and Priyalal S.Wijewarnasuriya, " Multispectral EO/IR sensor model for evaluating UV, visible, SWIR, MWIR and LWIR system performance" Proceedings of SPIE 7300, 73000H (2009)

[3] Abdiel Rivera, John Zeller, Tariq Manzur, Ashok Sood and Mehdi Anwar, " MOCVD Growth and Characterization of ZnO Nanowire Arrays for UV Detectors" Proceedings of SPIE , Volume 8540, October 2012.

[4] Liang, S., Sheng, S., Liu, Y., Huo, Z., Lu, Y., and Shen, H., "ZnO Schottky ultraviolet photodetectors," J. Cryst. Growth 225, 110-113 (2001).

[5] Zhang, J., Que, W., Jia, Q., Ye, X., and Ding, Y., "Controllable hydrothermal synthesis of ZnO nanowires arrays on Al-doped ZnO seed layer and patterning of ZnO nanowires arrays via surface modification of substrate," Appl. Surf. Sci. 257(23), 10134-10140 (2011).

[6] Lee, C. H., Yi, G. C.., Zuev, Y. M., and Kim, P., "Thermoelectric power measurements of wide band gap semiconducting nanowires,"Appl. Phys. Lett. 94, 22106 (2009).

[7] Falyouni, F., Benmamas, L., Thiandoume, C., Barjon, J., Lusson, A., Galter, P., and Sallet, V., "Metal organic chemical vapor deposition growth and luminescence of ZnO micro- and nanowires," Journal Vac. Sci. Technol. B 87, 1662 (2009).

[8] Jeong, M. C., Oh, B.Y., Lee, W., and Myoung, J. M., "Comparative study on the growth characteristics of ZnO nanowires and thin films by metal-organic chemical vapor deposition (MOCVD)," Journal of. Crystal Growth 268, 149-154 (2004).

[9] Kim, S. W., Fujita, S., and Fujita, S., "ZnO nanowires with high aspect ratios grown by metal-organic chemical vapor deposition using gold nanoparticles," Appl. Phys. Lett. 86,153119 (2005).

[10] Lee, W., Jeong, M. C., and Myoung, J. M., "Catalyst-free growth of ZnO nanowires by metal-organic chemical vapor deposition (MOCVD) and thermal evaporation," Acta Mat. 52, 3949-3957 (2004).

[11] Liou, S. C., Hsiao, C. S., and Chen, S. Y., "Growth behavior and microstructure evolution of ZnO nanorods grown on Si in aqueous solution," Journal of. Crystal. Growth 274, 438 (2005).

[12] Dong, J. W., Osinski, A., Hertog, B., Dabiran, A. M., Chow, P. P., Heo, Y. W., Norton, D. P, and Pearton, S. J., "Development of MgZnO-ZnO-AlGaN heterostructures for ultraviolet light emitting applications," J. Electron. Mat. 34, 416-423 (2005).

[13] Rivera, A., Zeller, J., Sood, A.K., and Anwar, A. F. M., "A Comparison of ZnO Nanowires and Nanorods Grown Using MOCVD and Hydrothermal Processes," J. Electron. Mat. 42, 894-900 (2013).

[14] Ha, B., Ham, H., and Lee, C. J., "Photoluminescence of ZnO nanowires dependent on O_2 and Ar annealing," Phys. Chem. Solids 69, 2453-2456 (2008).

[15] Djurišić, A. B., Ng, A.M.C., and Chen, X.Y., "ZnO nanostructures for optoelectronics: Material properties and device applications," Progress Quantum Electronics 34, 191-259 (2010)

[16] Mehdi Anwar, Abdiel Rivera, Anaz Mazady, Hung Chou, John Zeller and Ashok K. Sood, "ZnO Solar Blind Detectors: from Material to System", Proceedings of SPIE Volume 8868, 8868B (2013).

[17] R. Blackwell, D. Lacroix, T. Bach, et. al " 17 micron microbolometer FPA Technology at BAE Systems" Proceedings of SPIE, Volume 7298,72980P (2009).

[18] C. Li, G. Skidmore, C. Howard, E. Clarke and J. Han, "Advancement in 17-micron pixel pitch uncooled focal plane arrays" Proceedings of SPIE, Volume 7298, 72980S (2009).

[19] T. Schimert, C. Hanson, J. Brady, et. al. " Advanced in small-pixel, large-format alpha-silicon bolometer arrays" , Proceedings of SPIE, Volume 7298, 72980T (2009)

[20] C. Trouilleau, B. Fieque, S. Noblet, F. Giner et.al. "High Performance uncooled-amorphous silicon TEC less XGA IRFPA with 17 micron pixel pitch" Proceedings of SPIE Volume 7298, 72980Q, (2009).

[21] E. Pop, D. Mann, Q. Wang, K. Goodson, H. Dai, Thermal Conductance of an Individual Single-Wall Carbon Nanotube above Room Temperature Nano Letters 6, 96 (2006)

[22] A. Akturk, N. Goldsman, G. Metze, "Self-consistent modeling of heating and MOSFET performance in 3-D integrated circuits," IEEE Trans. on Elect. Dev. 52 (11): 2395-2403 (2005).

[23] Ashok K. Sood, E. James Egerton, Yash R. Puri, Gustavo Fernandes, Jimmy Xu, Akin Akturk, Neil Goldsman, Nibir K. Dhar, Madan Dubey, Priyalal S. Wijewarnasuriya and Bobby I Lineberry, " Design and Development of CNY based Micro-bolometer for IR Imaging Applications" Proceedings of SPIE, Volume 8353, 83533A , May 2012

[24] Gustavo Fernandes, Jin Ho Kim, Jimmy Xu, Ashok K. Sood, Nibir K. Dhar and Madan Dubey, " Unleashing Giant TCR from Phase –Changes in Carbon Nanotube Composites" Proceedings of SPIE Volume 8868, 88680S , September 2013

[25] Rongtao Lu, Jack J. Shi, F. Javier Baca and Judy Z. Wu, "High Performance Multiwall Carbon Nanotube Bolometer" Journal of Applied Physics, 108, 084305 (2010).

[26] Rongtao Lu, Rayyan Kamal and Judy Z. Wu, " A comparative study of 1/f noise and temperature coefficient of resistance in multiwall and single-wall carbon nanotube bolometers" nanotechnology, Volume 22, 265503 (2011).